Effect of zinc doping on electrical properties of LaAlO$_3$ perovskite

Anastasia V. Egorova[ab*], Ksenia G. Belova[ab], Irina E. Animitsa[ab],
Yelizaveta A. Morkhova[cd], Artem A. Kabanov[ce]

a: Ural Federal University, 19 Mira St., Yekaterinburg, 620075, Russia
b: Institute of High Temperature Electrochemistry, Ural Branch Russian Academy of Sciences,
   20 Akademicheskaya St., Yekaterinburg, 620219, Russia
c: Samara Center for Theoretical Materials Science (SCTMS), Samara State Technical University,
   12 Novo-Sadovaya St., Samara, 443110, Russia
d: Samara Center for Theoretical Materials Science (SCTMS), Samara University,
   1 Academician Pavlov St., Samara, 443110, Russia
e: P. N. Lebedev Physical Institute of the Russian Academy of Sciences,
   221 Novo-Sadovaya St., Samara, 443011, Russia
* Corresponding author: Anastasia.Obrubova@urfu.ru

This article belongs to the PCEE-2020 Special Issue.

Abstract

New solid solution with the general formula of LaAl$_{1-x}$Zn$_x$O$_{3-1/2x}$ was prepared by a solid-state reaction route. According to XRD, the crystal structure of LaAlO$_3$ is rhombohedral, while the solid solution possesses cubic symmetry. Homogeneity region of the solid solution LaAl$_{1-x}$Zn$_x$O$_{3-1/2x}$ was narrow and limited to the maximum concentration of 5 mol. %. Computer simulations using crystallochemistry and density functional theory approaches showed that LaAlO$_3$ has high energy barriers for O^{2-}-ion transport (>2.79 eV). These results are in good agreement with the low values of electrical conductivity obtained experimentally. The electrical conductivity of LaAl$_{1-x}$Zn$_x$O$_{3-1/2x}$ was measured by impedance spectroscopy in the temperature range of 200–1000 °C. The partial substitution of Al^{3+} by Zn^{2+} was found to increase the electrical conductivity by ~2 orders of magnitude. The electrical conductivity of doped phase LaAl$_{0.95}$Zn$_{0.05}$O$_{2.975}$ as a function of oxygen partial pressure was measured, and the partial contributions (oxygen-ionic and electronic) were determined. It was found that the sample has mixed ionic and p-type electronic conductivity, while the electronic contribution increases with the rise of the temperature.

1. Introduction

During the past few decades, the perovskites have been used in various electrochemical devices and their properties have been well described. For example, these materials are promising electrolyte systems for solid oxide fuel cells (SOFCs). The general requirements for an electrolyte are high ionic conductivity, stability in both oxidizing and reducing environments, good mechanical properties and long-term stability. The electrolyte system, namely, yttria stabilized zirconia (YSZ) has been widely investigated for SOFCs, operating at 900–1000 °C [1]. In recent years, the focus of SOFC development has been on lowering the operating temperatures. Perovskites A^{+2}B^{+4}O$_3$, for example

doped BaCeO$_3$ and BaZrO$_3$, are promising materials in this field due to their high proton conductivity. However, the presence of an alkaline earth component in the composition of perovskites A^{+2}B^{+4}O$_3$ can result in the formation of the corresponding carbonates [2–5], and thus to the degradation of the material.

A new direction of materials development is "alkaline earth elements free strategy", that is, investigation of compounds not containing an alkaline-earth component. The modification of compounds with the general formula of A^{3+}B^{3+}O$_3$ is the most simple implementation of this approach [6–9].

The lanthanum aluminate LaAlO$_3$ (LAO) can be a promising perovskite material in this trend due to its high

chemical stability [10–13]. The systems based on $LaAlO_3$ can be good ionic or mixed conductors by adding suitable dopants [12]. Aluminates based on $LaAlO_3$ have such advantages as low cost of the initial materials, high thermodynamic stability due to the strength of Al–O bonds and wide T–$p(O_2)$ regions of ionic conductivity [12].

Complex oxide $LaAlO_3$ is a tolerant system to the different substitutions. The possibility of introducing various dopants into the La^{3+} or Al^{3+} –sublattices of $LaAlO_3$ has been proven in several works. The substitutions of lanthanum by alkaline-earth elements (Ca, Sr, Ba) [7,11,14,15], aluminum by magnesium [7,15,16], and simultaneous co-substitutions into both sublattices [7–9,12,13,15,16] have been made. Thus, it was shown that the acceptor doping of $LaAlO_3$ produces a deficiency in the oxygen sublattice and, respectively, induces oxygen-ionic transport. It should be noted that the main substitutions are performed for the La-sublattice, and in this case the alkaline earth metal is the dopant, which reduces the chemical resistance of the material.

In this study we used ZnO as a dopant for several reasons: i) as an acceptor dopant, divalent Zn^{2+} increases the concentration of oxygen vacancies in the perovskite-lattice; ii) in addition, due to the stable oxidation state, the doping will not lead to an increase in the electronic conductivity; iii) zinc belongs to the IIB group in the Periodic Table, it is not an alkaline earth element, the presence of which impairs chemical stability. Also, we assume that the introduction of zinc can reduce the synthesis temperature and will make it possible to obtain dense ceramics, as it was found in the works [17–20].

Although lanthanum aluminate has been a subject of many studies, the data of its electrical properties are not in good agreement. Thus, it is necessary to systematize the data on the electrical properties of $LaAlO_3$. In the present study, we also calculated migration paths and migration energy barrier for oxygen transport. The investigations of electrical properties of $LaAlO_3$ and Zn-doped at the B-site $LaAlO_3$ were performed.

2. Experimental

The $LaAl_{1-x}Zn_xO_{3-1/2x}$ (where x=0, 0.05, 0.1, 0.15, 0.33) samples were synthesized by solid state method. As initial reagents, preliminary dried oxides of the corresponding elements (99.99% purity, REACHIM, Russia) were used. Aluminum and zinc oxides were dried at 500 °C for 3 h to remove adsorption water. Lanthanum oxide was calcined at 1100 °C for 3 h to decompose the lanthanum carbonates $LaOHCO_3$ and $La_2O_2CO_3$ in accordance with [21].

The stoichiometric amounts of the oxides were weighed on an analytical balance with an accuracy of ±0.0001 g, mixed and ball-milled in ethanol. The synthesis was started at 700 °C, then the temperature was increased stepwise by 100 °C. All heat treatment steps were carried out with an isothermal holding time of 24 h, cooling with a

furnace. After each heat treatment, the samples were milled in a planetary ball mill Pulverisette 6 (Fritsch, Germany) with ethanol and with using the zirconia milling bodies.

Single phase aluminate $LaAlO_3$ was obtained at 1250 °C. Single phase doped aluminate $LaAl_{0.95}Zn_{0.05}O_{2.975}$ was obtained at lower temperature 1200 °C. The synthesis of the samples $LaAl_{1-x}Zn_xO_{3-1/2x}$ (x=0.1, 0.15, 0.33) were continued at higher temperature 1300 °C. However, these samples were not obtained as the single phases; also, the sample with x = 0.33 was melted at high temperatures.

Phase composition of the samples was determined by a powder X-ray diffraction method using a diffractometer D8 Advance (Bruker) with Cu Kα radiation in increments of 0.05θ in the range of angles 2θ=10°–120° with exposures of 1s, a voltage of 40 kV and a current of 40 mA. The refinement of unit cell parameters was made using the FullProf software [22].

The surface morphology of the powder samples was studied by means of a high-end imaging desktop scanning electron microscope the Thermo Scientific "Phenom" Pharos (Phenom-World, Netherlands) with FOV: 912 μm, mode: 15kV - map, detector: BSD Full.

Multi-method modeling for the oxygen-ion conductivity for pure lanthanum aluminate $LaAlO_3$ was performed. We used a combined approach consisting of a crystallochemical analysis of geometric characteristics of free space in crystals, simulation of oxygen transport by the bond valence method (BVSE method) and quantum-chemical modeling of the ionic conductivity within the density functional theory (DFT) method.

The geometrical-topological approach is based on the Voronoi partition [23] and is implemented in the ToposPro software package [24]. Crystallochemical analysis reveals the geometric capabilities of the structure, i.e. a presence of wide voids and channels, which are accessible for anion migration. The criterion R_{chan} (an elementary channel radius) was determined for the geometrical analysis, which characterizes the presence of voids and channels in the structure, as described in [25]. R_{chan} describes the width of the bottleneck between two voids. This criterion is the sum of the radii of the working ions and the environment ions, taking into account the coefficient of ion deformation. This coefficient also takes into account the polarizability of the migration ion when passing through the channel. Based on the set of well-known oxygen conductors, we have chosen the coefficient of deformation for oxygen conductors of 0.8, so that R_{chan} was assumed to be equal to 1.73 Å.

The quantitative semi-empirical evaluation of activation energies of oxygen diffusion was conducted by the bond valence method. This approach is implemented in the SoftBV [26] and 3DBVSMAPPER [27] packages. We use the SoftBV software package developed by the Adams group [26], due to its availability to users. The calculation procedure was carried out as described in [26]. We calculated

the migration energies for each species in the structure. This made it possible to reveal that ionic conductivity in LaAlO₃ is due only to oxygen anions. The method is not accurate enough, but allows a quick initial assessment of activation energies for ranking and, next, more precise quantum-chemical modeling of ion transport as described by Nestler et al. [28].

The DFT-calculations were performed for structure relaxation and calculations of oxygen migration energies. The VASP package [29] with the Nudged Elastic Band (NEB) method [30] were utilized. The GGA (generalized gradient approximations) exchange-correlation functional in the form of PBE (Perdew-Burke-Ernzerhof) [31] was applied. When optimizing the structure, the convergence thresholds were used 10^{-6} eV and 10^{-5} eV/Å for the energy and interatomic forces, respectively. The cutoff energy of plane waves in all calculations was taken equal to 600 eV and uniform Γ-centered k-point mesh for sampling the Brillouin zone with a reciprocal-space resolution of $2\pi \times 0.025$ Å^{-1} was used. To minimize periodic interactions between neighboring cells, a 2×1×1 supercell was used for NEB calculations. The optimized supercell lattice parameters are $a = b = 10.817$ Å, $c = 13.182$ Å, and $V = 1335.924$ Å^3. The convergence threshold for ion optimization was 10^{-2} eV/Å for NEB calculations. NEB calculations were carried out with a fixed supercell with parameters that corresponded to the optimized values.

The theoretical results were compared with the experimentally investigated electrical properties. For electrical measurements, the powder samples were formed into pellets with 10–12 mm in diameter and ~2 mm thickness by pressing at ~50 MPa. A solution of rubber in hexane was used as a plasticizer. The pellets were sintered at the temperature of 1250 °C (LaAl$_{1-x}$Zn$_x$O$_{3-1/2x}$) and 1650 °C (LaAlO₃) for 24 h. Platinum electrodes in the form of finely dispersed paste mixed with an alcohol solution of rosin were applied to the preliminarily polished surfaces of the sintered tablets. The electrodes were burned for 2 h in air at 900 °C.

The relative density of the samples, determined by a hydrostatic method, was found to be 96% (LaAl$_{0.95}$Zn$_{0.05}$O$_{2.95}$) and 91% (LaAlO₃). For this experiment, dried pellets were soaked in kerosene (ρ_k=0.8 g/cm³) for 24 hours. For the calculations, the mass of dried samples (m_{dry}) and the mass of pellets saturated of kerosene (m_{sat}) were used according to the equation:

$$W = \frac{m_{sat} - m_{dry}}{m_{dry}} \cdot \frac{\rho_{H_2O}^{20}}{\rho_k} \qquad (1)$$

The conductivity of the samples was characterized by an impedance spectroscopy technique. Measurements were performed by the two-probe method using a Z–1000 P (Elins) impedance spectrometer under varying temperature (200–1000 °C) and partial pressures of oxygen (pO₂ = 1·10^{-20} – 0.21 atm). The oxygen partial pressure was measured and controlled by an oxygen sensor and a

pump made of a solid electrolyte based on yttrium-stabilized zirconia ZrO₂(Y₂O₃).The obtained impedance spectra were analyzed using an equivalent circuits method and refined using Zview software [32].

3. Results and Discussion

3.1. Structural features of LaAlO₃ and morphology characterization

The XR-diffractogram of LaAlO₃ is presented in the Supplementary (Fig. S1). The obtained phase LaAlO₃ is characterized by the rhombohedral structure, in accordance with the JCPDS card №31-0022 and in agreement with literature data [6,8,10,33]. This is a slightly distorted cubic perovskite with the sp.gr. $R\overline{3}c$ and the unit cell parameters: $a = 5.408(5)$ Å, $c = 13.182(3)$ Å, $\gamma = 120°$. Rhombohedral structure is stable modification of LaAlO₃ at room temperature. However, lanthanum aluminate exhibits a reversible phase transition from rhombohedral to cubic symmetry at heat treatment above 400 °C [34–36]. The cubic phase is unstable under room temperature. But in some studies, the cubic structure was stabilized at room temperature. A cubic modification was obtained by the mechanochemical [11] and the Pechini methods [15].

The morphology of the sample was investigated using scanning electron microscopy (SEM). Fig. S2*a* shows the SEM image of the powder sample LaAlO₃. The grains of the sample were small and had a size of ~1 µm.

Below we present the theoretical calculations of migration paths and a migration energy barrier for the oxygen conductivity for the rhombohedral phase LaAlO₃, obtained in this work.

3.2. Theoretical study of O²⁻-ion conductivity

Voronoi partition was built for LaAlO₃ using the above described criterion R_{chan} in the ToposPro program. We have found a three-dimensional migration map for oxygen anions in the structure (Fig. 1).

The migration energy barrier for oxygen ion diffusion in LaAlO₃ is 1.844 eV according to the BVSE modeling, the corresponding energy profile is shown in Fig. S3. BVSE predict the formation of a three-periodic migration map.

The DFT results show that the oxygen diffusion map consists of two independent paths (Fig. 2*a*), while only one path (Path 1) is enough for the 3D oxygen diffusion.
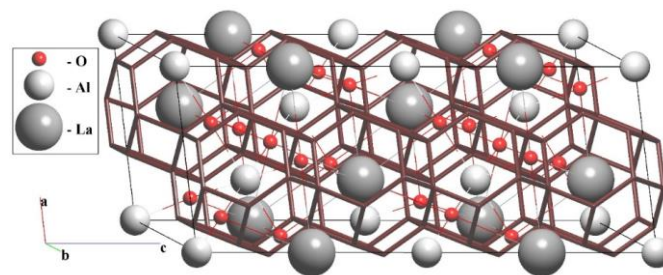
Fig. 1 Migration map for oxygen anions in LaAlO₃ according to the geometrical-topological analysis. 3D migration map is highlighted in brown.
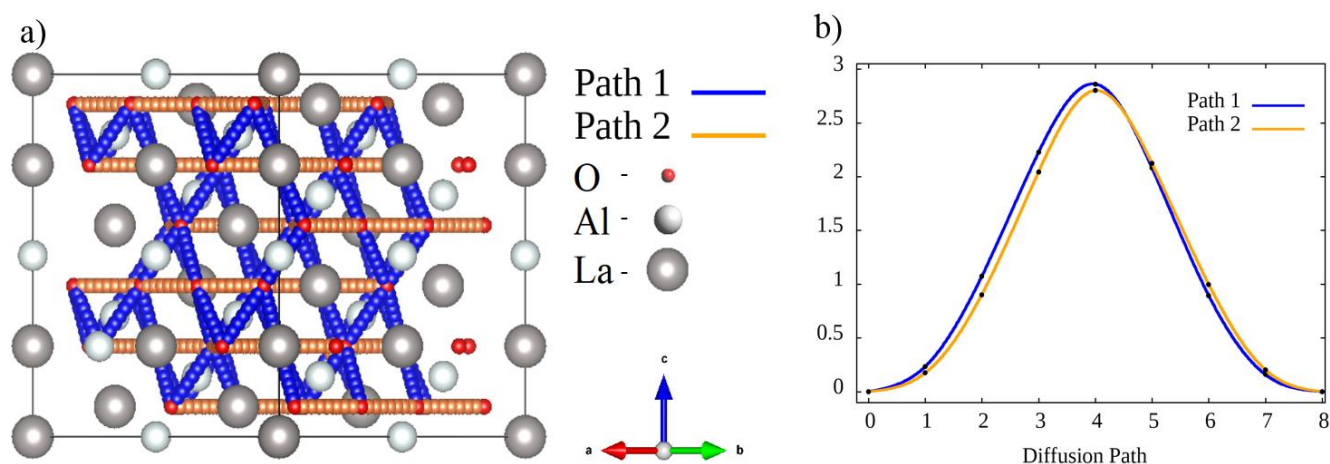
Fig. 2 The 3D oxygen diffusion map within 2×1×1 LaAlO$_3$ supercell according to the DFT-NEB results (a). Bonds between the atoms are not shown. The NEB results for the migration energy profiles for Path 1 and Path 2 (b).

The DFT-NEB migration energy barriers for the paths 1, 2 are 2.86 and 2.79 respectively, the energy profiles are shown in Fig. 2b. It should be noted that the DFT migration energy values surpass the BVSE ones, similar to already described in the Nestler et al. [28]. It can be caused by strong O-O repulsion as well as many-body effects, which are counted in DFT and not considered in BVSE. But quantitatively both methods provide the similar outlook for oxygen diffusion map as shown in Fig. 3. The oxygen vacancy formation energy was evaluated as 6.15 eV/site according to the DFT data, see the Supplementary for more details. Because of the activation energy for diffusion is usually considered as a sum of the vacancy formation energy and the migration energy, we may conclude that LaAlO$_3$ should have a poor oxygen conductivity due to very high barriers.

As known from the literature, the energy involved in the process of migration from one site to the unoccupied equivalent site must be low, certainly less than about 1eV [37]. The high quantitative values of the oxygen migration energy prove the necessity of doping perovskite in order to improve the conductive properties. Nevertheless, the implementation of a three-periodic migration map of O^{2-}-anion with the ability to migrate in different directions demonstrates the prospect of creating new perovskites with increased conducting properties.

Computer simulations using crystalochemistry and density functional theory approaches showed that LaAlO$_3$ has high energy barriers for O^{2-}-ion transport (>2.79 eV). However, computer simulations are carried out for ideal crystals, in according to the occupancy of all atoms at their sites. Therefore, the value of the experimental energy barrier can be less than the theoretical one due to defects and random vacancies in the real crystal.

3.3. Structural features of LaAl$_{1-x}$Zn$_x$O$_{3-1/2x}$ solid solution and morphology characterization

The formation of LaAl$_{1-x}$Zn$_x$O$_{3-1/2x}$ solid solution was controlled by XRD. Homogeneity region of the solid solution
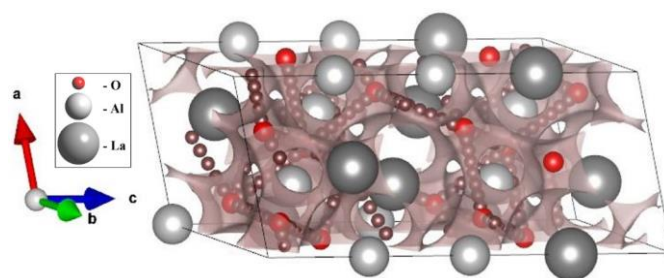
Fig. 3 A comparison between the BVSE oxygen diffusion pathways (shown by grey isosurfaces) and the DFT paths (tightly connected brown balls). 3D migration map is highlighted in brown.

LaAl$_{1-x}$Zn$_x$O$_{3-1/2x}$ was narrow and limited to the maximum concentration of 5 mol. %. The XRD pattern of the single phase LaAl$_{0.95}$Zn$_{0.05}$O$_{2.95}$ is presented in the Supplementary (Fig. S4.). At the same time, the sample with x = 0.1 is characterized by the presence of insignificant amount of the impurities of the starting reagents.

The structures of LaAl$_{0.95}$Zn$_{0.05}$O$_{2.975}$ (LAZ9505) and LaAl$_{0.9}$Zn$_{0.1}$O$_{2.95}$ (LAZ91) can be refined as cubic perovskites with the unit cell parameters of a = 3.785(2) Å and a = 3.779(9) Å, respectively (a $Pm\bar{3}m$ sp.gr.). The presence of zinc in the composition of solid solutions stabilizes the cubic structure of LaAlO$_3$.

Fig. S2b shows the SEM image of the powder sample LaAl$_{0.9}$Zn$_{0.1}$O$_{2.95}$. It can be seen that the sample has the same morphology as undoped sample. The grains of the sample had a size of ~1 μm and some grains aggregated to the clusters with the size of 10–20 μm.

3.4. Electrical measurements

Electrical properties were studied by the method of electrochemical impedance. As an example, for the sample of x = 0.05 the impedance spectra, recorded at different temperatures, were shown in Fig. 4a. The impedance plot is represented by one distorted semicircle started from the zero point. The impedance spectra were analyzed through the data fitting, using equivalent elementary circuits arranged in series consisting of one resistance (R) and one constant phase element (CPE) in parallel. The capacitance
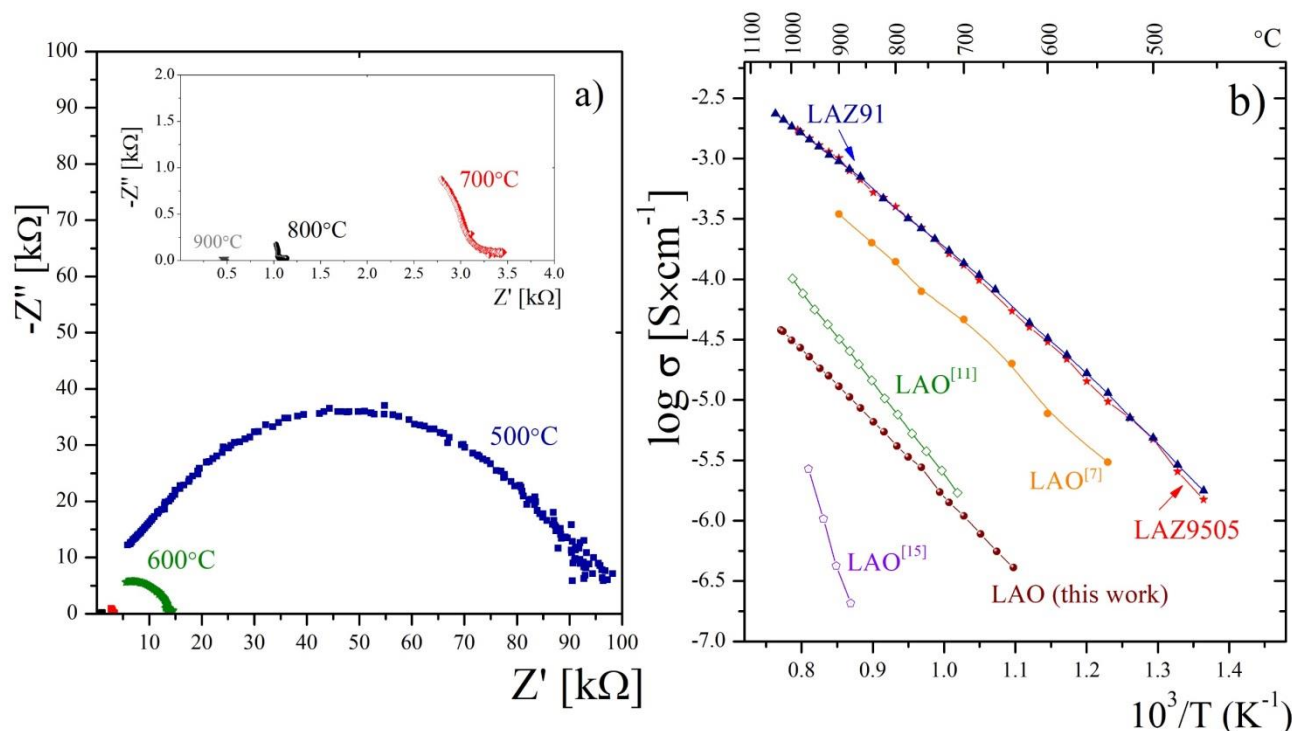
Fig. 4 Electrical measurements $LaAl_{1-x}Zn_xO_{3-1/2x}$: The impedance spectra of $LaAl_{0.95}Zn_{0.05}O_{2.975}$, recorded at 500–900 °C (a). Temperature dependences of conductivities of $LaAl_{1-x}Zn_xO_{3-1/2x}$ (x = 0.0, 0.05, 0.1), including literature data for comparison (b).

for these semicircles is determined to be $\sim10^{-11}$ F/cm. The results of electrical measurements showed that there is not difference in the general view of the impedance spectra of doped and undoped samples. We can assume that this semicircle corresponds to a bulk response. We made this conclusion on the basis of the comparison with the data, presented in [11], since in many respects we have similar results : i) the average grain size of $LaAlO_3$ was found to be ~1 μm ; ii) the capacitance for high-frequency semicircle is determined to be $\sim10^{-11}$ F/cm ; iii) the values of the conductivity of the undoped samples agree well (Fig. 4b).

The observed small second semicircle at low frequencies can be attributed to the grain boundary response. It should be said, according to literature data, the Nyquist plots are typical for the doped $LaAlO_3$ and exhibit, as usual, two semicircles – the bulk and grain boundary responses. However, the grain boundary resistance is very different from different works, and there is often a situation where the grain boundary semicircle is higher than the resistance of the bulk semicircle. For the investigated Zn-doped composition the observed second semicircle with specific capacitance of $\sim2\times10^{-9}$ F/cm was small and was visible as separate semicircle at higher temperatures (Supplementary Fig. S5a). The capacity calculated for this semicircle correlated well with the data presented in [11], where the same second semicircle was assigned to the grain boundary response too. The evolution of impedance spectra for different temperature ranges is shown in Fig. S5 and Fig. S6.

The comparison of data on conductivity and density for the ceramics based on aluminate $LaAlO_3$ is presented in the Table S1. As seen, the reported conductivity values scatter in a wide range; this implies a strong influence of the phase and elemental impurities, porosity and microstructural characteristics.

Fig. 4b compares the temperature dependences of conductivities of undoped $LaAlO_3$, prepared in this work with literature data [5,6,10], solid solution LAZ9505 and composition LAZ91. The samples LAZ9505 and LAZ91 showed a high conductivity. The pure $LaAlO_3$ exhibits a low ionic conductivity due to the high binding strength of Al–O [12]. These data for $LaAlO_3$ are in good agreement with the literature data, presented in [11], although the reported conductivity values scatter in a wide range (Fig.4b). Some literature data demonstrate a strong contribution of grain boundary resistivity to the total resistivity. For the reasons mentioned above, the bulk properties could not be determined and total contribution (bulk+grain boundary) has been presented [15]. At the same time, the high values of conductivity, measured in [7], are probably doubtful due to incorrect extrapolation of the large semicircle to the high frequencies.

Acceptor-doping of aluminum by zinc leads to an increase by 2 orders of magnitude of the total conductivity over the investigated temperature range. The energies of activation for LAZ9505 and LAO were 1.054 eV and 1.21 eV, respectively. This increase in conductivity of doped sample is due to creation of oxygen vacancies. The substitution of a divalent cation for a trivalent cation produces oxygen vacancy according to the quasichemical equation:

$$2ZnO \xrightarrow{Al_2O_3} 2Zn'_{Al} + 2O^{\times}_O + V^{\bullet\bullet}_O \qquad (2)$$
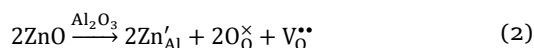
Fig. 5a shows the results of the measurements of the conductivity of the sample LAZ9505 as function of oxygen partial pressure in the temperatures range of 500–900 °C. Two areas can be distinguished on the isotherms: a region of electrolytic conductivity as a plateau (i.e. a region where conductivity does not depend on oxygen pressure, $pO_2 < 10^{-5}$ atm), and a region at high partial oxygen pressures ($pO_2 > 10^{-5}$ atm) for which a positive slope of the dependence is observed.

For $pO_2 < 10^{-5}$ atm and the electroneutrality condition $[Zn'_{Al}]=2[V^{\bullet\bullet}_O]$, the concentration of oxygen vacancies is fixed by the doping level, and pO_2-independent oxygen-ionic conductivity can be observed.

Incorporation of oxygen into the perovskite lattice with increasing pO_2 is accompanied by generation of electron-holes and is expressed by the equation:

$$V^{\bullet\bullet}_O + \frac{1}{2}O_2 \leftrightarrow O^{\times}_O + 2h^{\bullet} \qquad (3)$$
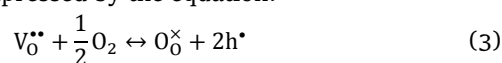
It is well established in the literature that doped LaAlO$_3$ is a p-type mixed conductor under oxidizing conditions [34], and LaAlO$_3$ phase exhibits ~10% oxygen-ionic transport numbers in air [34]. Accordingly, doping with zinc didn't change the general character of the conductivity of this phase.

A comparison of the oxygen-ion conductivities of the investigated sample LaAl$_{0.95}$Zn$_{0.05}$O$_{2.975}$ with an undoped composition LaAlO$_3$, as well as the most conductive composition of a Ca-doped sample, described in [11], is shown in Fig. 5b. As can be seen, doping in both cases leads to an increase in oxygen-ion conductivity, which is a result of the formation of oxygen vacancies (Eq. 3). However, the effect of increasing the oxygen-ionic conductivity upon doping with Ca^{2+} is greater. As it is known, two factors determine ionic conductivity, that is, defect concentration and mobility. For the case under consideration, with comparable defect concentrations, obviously, the mobility of oxygen vacancies is different. There are many factors that

affect the mobility of oxygen vacancies [38], and in the general case, expansion of the cell volume weakens the metal-oxygen bonding and increases the oxygen vacancy mobility [39]. We believe that due to the smaller lattice parameter and, as a consequence of the smaller volume of the unit cell (V_{cell}= 54.225 Å), the ionic conductivity of the Zn-doped sample is lower than that of the Ca-doped composition (V_{cell}= 54.483 Å) [11].

The oxygen-ionic transport numbers t_{ion} were calculated as a ratio of ionic conductivity to total conductivity $\sigma_{ion}/\sigma_{total}$. As an example, the Fig. 5c shows calculated data of t_{ion} vs. pO_2 for LaAl$_{0.95}$Zn$_{0.05}$O$_{2.975}$ at 500 °C. It was shown that maximum values of ~1 were reached at the partial oxygen pressures $pO_2 < 10^{-5}$ atm. The dependences of the oxygen-ion transport number vs. pO_2 at different temperatures were similar. As can be seen, the sample in air had ion transport numbers of about 20%. These results show that studied phase is mixed ionic-electronic conductor under oxidizing conditions. As for the comparison of the ion transport numbers with other doped phases, based on LaAlO$_3$, it is known that an increase in the ion transport numbers can be achieved with an increase in the concentration of the acceptor dopant (due to an increase in the concentration of oxygen vacancies). For example, for the most conductive aluminate-based phases La$_{1-x}$Ca$_x$AlO$_{3-\delta}$, when calcium is introduced from 5 mol. % to 15 mol. %, the ion transport numbers in air increase from 18% to 55% [11]. Thus, for low concentrations of the dopants (5 mol. %), the ion transport numbers are comparable and do not exceed 20%. Unfortunately, Zn-substituted solid solutions with a high concentration of the dopant are not formed; therefore, such doping does not allow a significant increase in the ion transport numbers. However, it should be noted that Zn-doping significantly lowered the sintering temperature of ceramics (1250 °C), for example, Ca-doped ceramics were obtained at 1450 °C [11]. Probably, in the future, codoped phases may be of interest.
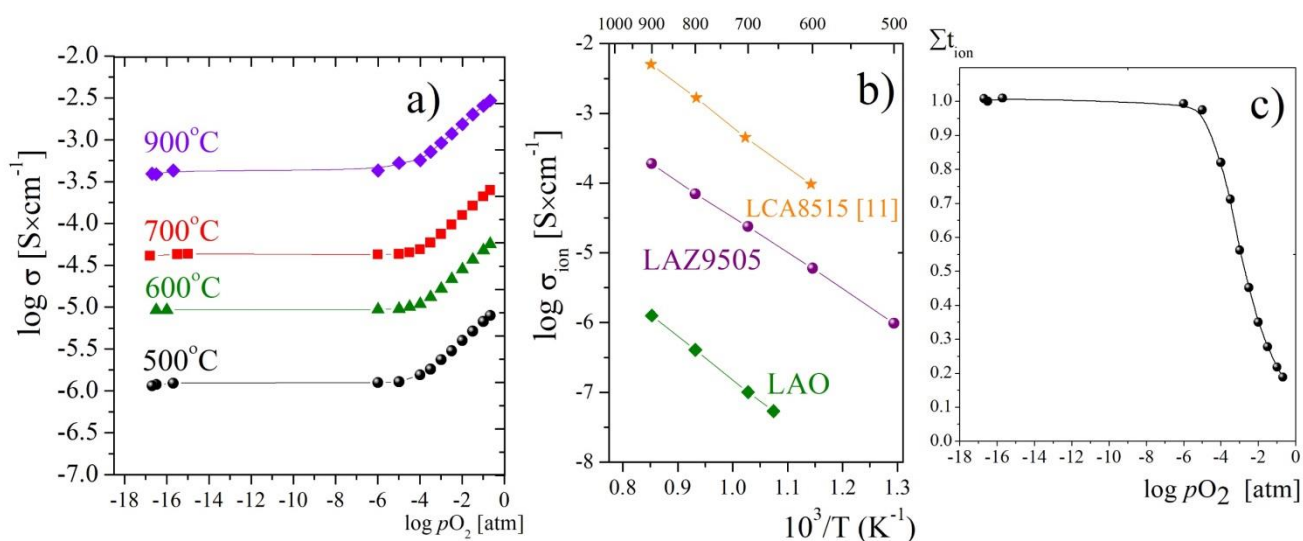
Fig. 5 Oxygen partial pressure dependence of conductivity of LAZ9505 at 500–900 °C (a); oxygen-ion conductivities of the LAZ9505, LAO and LCA8515 [11] samples (b); oxygen partial pressure dependence of oxygen-ion transport numbers of LAZ9505 at 500 °C (c).

For example, the codoping of Sr^{2+} + Mg^{2+} can significantly increase the conductivity, but high temperatures are required to obtain ceramics (Table S1). Therefore, the introduction of low concentrations of Zn^{2+} into the B-sublattice of $LaAlO_3$ whith simultaneous acceptor doping of the A-sublattice is a promising method for further investigations.

4. Conclusions

Zn-substituted $LaAl_{1-x}Zn_xO_{3-1/2x}$ perovskites were prepared by solid state method. XRD analyses showed the formation of single phase after annealing at 1250 °C for pure $LaAlO_3$ and 1200 °C for $LaAl_{0.95}Zn_{0.05}O_{2.975}$ sample. It was found that lanthanum aluminate has a small homogeneity region ($x \leq 0.05$). $LaAlO_3$ structure can be refined as rhombohedral and solid solution $LaAl_{0.95}Zn_{0.05}O_{2.975}$ crystallized in cubic symmetry, so, zinc-doping stabilized the cubic structure of $LaAlO_3$.

For rhombohedral phase $LaAlO_3$ migration paths and migration energy barrier for oxygen transport were calculated. The material reveals very high energy barriers (2.86 and 2.79 eV) of O^{2-}–ion transport and low conductivity. However, substitution by zinc was found to increase the electrical conductivity by 2 orders of magnitude compared to undoped $LaAlO_3$. Besides, sintering of Zn-doped phase at 1250 °C yielded dense ceramics with relative density of above 96%.

Acknowledgments

Supplementary materials

The supplementary data are available online at:
https://journals.urfu.ru/index.php/chimtech/article/downloadSuppFile/4746/726.

References

1. Jacobson AJ. Materials for Solid Oxide Fuel Cells. Chem Mater. 2010;22(3):660–74. doi:10.1021/cm902640j
2. Medvedev D, Murashkina A, Pikalova E, Demin A, Podias A, Tsiakaras P. BaCeO₃: Materials development, properties and application. Progress in materials science. 2014;60:72–129. doi:10.1016/j.pmatsci.2013.08.001
3. Sazinas R, Bernuy-Lopez C, Einarsrud M-A. Grande T. Effect of CO₂ exposure on the chemical stability and mechanical properties of BaZrO₃-ceramics. Journal of the American Ceramic Society. 2016;99:3685–95. doi:10.1111/jace.14395
4. Gopalan S, Virkar AV. Thermodynamic stabilities of SrCeO₃ and BaCeO₃ using a molten salt method and galvanic cells. J Electrochem Soc. 1993;140:1060–5. doi:10.1149/1.2056197
5. Medvedev D, Lyagaeva J, Plaksin S, Demin A, Tsiakaras P. Sulfur and carbon tolerance of BaCeO₃ – BaZrO₃ proton-conducting materials. Journal of Power Sources. 2015;273:716–23. doi:10.1016/j.jpowsour.2014.09.116
6. Zitouni H, Tahiri N, Bounagui O El, Ez-Zahraouy H. Electronic, transport and optical properties in perovskite compound LaGaO₃. Mater Res Express. 2020;7(3):035501. doi:10.1088/2053-1591/ab778c
7. Fung K-Z, Chen T-Y. Comparison of dissolution behavior and ionic conduction between Sr and/or Mg doped LaGaO₃ and LaAlO₃. J. Power Sources. 2004;132(1–2): 1–10. doi:10.1016/j.jpowsour.2003.12.062
8. Lybye D, Poulsen FW, Mogensen M. Conductivity of A- and B-site doped LaAlO₃, LaGaO₃, LaScO₃ and LaInO₃ perovskites. Solid State Ionics. 2000;128:91–103. doi:10.1016/S0167-2738(99)00337-9
9. Fung K-Z, Chen T-Y. A and B-site substitution of the solid electrolyte LaGaO₃ and LaAlO₃ with the alkaline-earth oxides MgO and SrO. Journal of Alloys and Compounds. 2004;368(1–2):106–115 doi:10.1016/j.jallcom.2003.08.059
10. Fung K-Z, Chen T-Y. Cathode-supported SOFC using a highly conductive lanthanum aluminate-based electrolyte. Solid State Ionics. 2011;188(1):64–8. doi:10.1016/j.ssi.2010.09.035
11. Fabián M, Arias-Serrano BI, Yaremchenko AA, Kolev H, Kaňuchová M, Briančin J. Ionic and electronic transport in calcium-substituted LaAlO₃ perovskites prepared via mechanochemical route. Journal of the European Ceramic Society. 2019;39(16):5298–308. doi:10.1016/j.jeurceramsoc.2019.07.038
12. Park JY, Choi GM. Electrical conductivity of Sr and Mg doped LaAlO₃. Solid State Ionics. 2002;154–155:535–40. doi:10.1016/S0167-2738(02)00510-6
13. Park JY, Choi GM. The effect of Ti addition on the electrical conductivity of Sr- and Mg-doped LaAlO₃. Solid State Ionics. 2005;176(37–38):2807–12. doi:10.1016/j.ssi.2005.09.007
14. Lima E, Villafuerte-Castrejón ME, Saniger JM, Ibarra-Palos A, Sánchez-Sánchez JE, Álvarez LJ. Experimental XRD and NMR, and molecular dynamics study of Sr containing LaAlO₃ perovskite. Solid State Ionics. 2008;178(39–40):1944–9. doi:10.1016/j.ssi.2008.01.036
15. Silva CA, Miranda PEV. Synthesis of LaAlO₃ based materials for potential use as methane-fueled solid oxide fuel cell anodes. International journal of hydrogen energy. 2015;40:10002–15. doi:10.1016/j.ijhydene.2015.06.019
16. Nguyen TL, Dokiya M, Wang S, Tagawa H, Hashimoto T. The effect of oxygen vacancy on the oxide ion mobility in LaAlO₃-based oxides. Solid State Ionics. 2000;130:229–41. doi:10.1016/S0167-2738(00)00640-8
17. Demchuk VA, Shchekina GB, Kostyukov NS. Effect of mineralizing additives ZnO and B₂O₃ on the sintering temperature of steatite ceramics, Russian Journal of Promising materials. 2013;6:11–4. https://www.elibrary.ru/item.asp?id=19079156
18. Sukhanov MV, Pet'kov VI, Firsov DB. Sintering mechanism of high density NZP-ceramics. Inorganic materials. 2011;47(6):674–8. doi:10.1134/S0020168511060197
19. Sizova AS, Popova NA, Lukin ES. Influence of temperature of synthesis on the properties of ceramics from magnesium oxide containing zinc oxide as a dependent additives. Advances in chemistry and chemical technology [Internet]. 2017 [cited 2020];31(3):105–7. Russian. Available from: https://cyberleninka.ru/article/n/vliyanie-temperatury-sinteza-prekursorov-karbonatov-na-svoystva-keramiki-iz-oksida-magniya-legiruemoy-oksidom-tsinka/viewer
20. Medvedev DA, Murashkina AA, Demin AK. Formation of Dense Electrolytes Based on BaCeO₃ and BaZrO₃ for Application in Solid Oxide Fuel Cells: The Role of Solid State Reactive Sintering. Review Journal of Chemistry. 2015;5(3):193–214. doi:10.1134/S2079978015030024
21. Bakiz B, Guinneton F, Arab M, Benlhachemi A, Villain S, Satre P, Gavarri J-R. Carbonatation and Decarbonatation Kinetics in the La₂O₃-La₂O₂CO₃ System under CO₂ Gas Flows. Advances in

Materials Science and Engineering. 2010;2010:1–6. doi:10.1155/2010/360597

22. Rodríguez-Carvajal J. An introduction to the program FullProf Version 2001. Laboratoire Léon Brillouin, CEA-CNRS, Saclay, France.

23. Blatov VA, Ilyushin GD, Blatova OA, Anurova NA, Ivanov-Schits AK, Dem'yanets LN. Analysis of migration paths in fast-ion conductors with Voronoi–Dirichlet partition. Acta Crystallographica Section B. 2006;62(6):1010–8. doi:10.1107/S0108768106039425

24. Blatov VA, Shevchenko AP, Proserpio DM. Applied Topological Analysis of Crystal Structures with the Program Package ToposPro. Crystal Growth & Design. 2014;14(7):3576–86. doi:10.1021/cg500498k

25. Blatov VA, Anurova NA. Analysis of ion-migration paths in inorganic frameworks by means of tilings and Voronoi-Dirichlet partition: a comparison. Acta Crystallographica Section B. 2009;65(4):426–34. doi:10.1107/S0108768109019880

26. Adams S, Rao, RP. High power lithium ion battery materials by computational design. Physica Status Solidi A. Applications and Materials Science. 2011;208(8):1746–53. doi:10.1002/pssa.201001116

27. Sale M, Avdeev M. 3DBVSMAPPER: a program for automatically generating bond-valence sum landscapes. Journal of applied crystallography. 2012;45(5):1054–6. doi:10.1107/S0021889812032906

28. Nestler T, Meutzner F, Kabanov AA, Zschornak M, Leisegang T, Meyer DC. Combined Theoretical Approach for Identifying Battery Materials: Al^{3+} Mobility in Oxides. Chemistry of Materials. 2019;31(3):737–47. doi:10.1021/acs.chemmater.8b03631

29. Kresse G, Furthmüller J. Efficient iterative schemes for ab initio total-energy calculations using a plane-wave basis set. Physical Review B. 1996;54(16):11169–86. doi:10.1103/PhysRevB.54.11169

30. Henkelman G, Jónsson H. Improved tangent estimate in the nudged elastic band method for finding minimum energy paths and saddle points. The Journal of Chemical Physics. 2000;113(22):9978–85. doi:10.1063/1.1323224

31. Perdew JP, Burke K, Ernzerhof M. Generalized Gradient Approximation Made Simple. Physical Review Letters. 1996;77(18):3865–8. doi:10.1103/PhysRevLett.77.3865

32. Johnson D, Inc. ZView: a Software Program for IES Analysis, Version 2.8. Scribner Associates: Southern Pines, NC; 2002. 200 p.

33. Alves N, Ferraz WB, Faria LO. Synthesis and investigation of the luminescent properties of carbon doped lanthanum aluminate ($LaAlO_3$) for application in radiation dosimetry. Radiation Measurements. 2014;71:90–4. doi:10.1016/j.radmeas.2014.02.008

34. Kilner JA, Barrow P, Brook RJ. Electrolytes for the high temperature fuel cell; experimental and theoretical studies of the perovskite $LaAlO_3$. Journal of Power Sources. 1978;3:67–80. doi:10.1016/0378-7753(78)80006-8

35. Benam MR, Abdoshahi N, Sarmazdeh MM. Ab initio study of the effect of pressure on the structural and electronic properties of cubic $LaAlO_3$ by density function theory using GGA, LDA and PBEsol exchange correlation potentials. Physica B. 2014;446:32–8. doi:10.1016/j.physb.2014.04.00609

36. Deren PJ, Lemanski K, Gagor A, Watras A, Maecka M, Zawadzki M. Symmetry of $LaAlO_3$ nanocrystals as a function of crystallite size. Journal of Solid State Chemistry. 2010;183:2095–100. doi:10.1016/j.jssc.2010.07.01

37. Skinner SJ, Kilner JA. Oxygen ion conductors. Materials Today. 2003;6(3):30–7. doi:10.1016/S1369-7021(03)00332-8

38. Ranlov J, Bonanos N, Poulsen FW, Mogensen M. Criteria for prediction of high oxide ion conductivity in perovskite oxides. Solid State Phenomena. 2003;39–40:219–22. doi:10.4028/www.scientific.net/SSP.39-40.219

39. Wakamura K. Ion conduction in proton- and related defect (super) ionic conductors: Mechanical, electronic and structure parameters. Solid State Ionics. 2009;180(26–27):1343–9. doi:10.1016/j.ssi.2009.08.009